IOSR Journal of Dental and Medical Sciences (IOSR-JDMS)
e-ISSN: 2279-0853, p-ISSN: 2279-0861.Volume 22, Issue 3 Ser.15 (March. 2023), PP 31-45
www.iosrjournals.org

Efficacy of Thymoquinone Loaded Chitosan Nanoparticles Coated by Hyaluronic Acid in Targeting Oral Squamous Cell Carcinoma: An *in-Vitro* Study

Hend A Alshabrawy [1]*, Mohamed H Amer [1], Sally S Mohammed [2], Wafaa H El-Hossary [1]

[a] *Oral Pathology Department, Faculty of Dentistry, Suez Canal University, Ismailia, Egypt*
[b] *Histology and Cell Biology Department, Faculty of Medicine, Suez Canal University, Ismailia, Egypt*
**corresponding auther*

Abstract:
Background: *The cell surface glycoproteins CD44, the main receptors for hyaluronic acid (HA), are highly expressed in most head and neck squamous cell carcinoma. Consequently, HA was used as a targeting ligand with different types of nanocarriers. This study aims to evaluate the efficacy of thymoquinone (TQ) loaded chitosan nanoparticles (CS-NPs) coated by HA in targeting oral squamous cell carcinoma.* ***Material and methods:*** *TQ-loaded CS NPs (TQ-CS NPs) and TQ-loaded CS NPs coated by HA (TQ-CS-HA NPs) were formed to evaluate the targeting ability of NPs coated by HA on human tongue squamous cell carcinoma and human normal oral epithelial cell lines. They were treated with different concentrations of free TQ, TQ-CS NPs, and TQ-CS-HA NPs. Cell viability was assessed with WST-1 assay after 24, 48, and 72h. The cellular uptake of TQ-CS-HA NPs was evaluated by confocal laser scanning microscope (CLSM) imaging.* ***Results:*** *viability of cancer cells was decreased after treatment with TQ-CS-HA NPs compared with free TQ, while normal cells showed better viability when treated with NPs especially TQ-CS-HA NPs after 72h. Morphological analysis of both cell lines by phase contrast microscope (PCM) showed signs of apoptotic, necrotic, and autophagic changes within the cells with various levels. The fluorescent intensity of TQ-CS-HA NPs was higher in the cancer cells than in normal cells after 3, and 4h as detected by CLSM.* ***Conclusion:*** *it can be concluded that surface coating of CS NPs by HA can effectively increase the targeting of the loaded drug to cancer cells and diminish toxicity on normal cells.*

Keywords: *Squamous cell carcinoma, thymoquinone, chitosan, hyaluronic acid, nanoparticles.*

Date of Submission: 11-03-2023 Date of Acceptance: 25-03-2023

I. Introduction

Head and neck squamous cell carcinoma (HNSCC) is the most frequent type of malignancy in the head and neck area especially in the oral cavity, pharynx, and larynx [1]. According to the global cancer statistics published in 2021, HNC represents 5% of all cancers, with nearly 900,000 new cases and 500,000 deaths reported annually. Lip and oral cancer constitute the 16^{th} most common malignancies with 377,713 new cases and 15^{th} cancer leading cause of death worldwide with 177,757 new deaths. The mortality of lip and oral cancer reach 48.5% in males and 53% in females [2]. Its incidence and mortality have a wide geographic variation around the world depending on gender, age groups, countries, ethnic groups, and socioeconomic status [3]. Oral squamous cell carcinoma (OSCC) is the most frequent type of oral cancer. The major applied treatments for the locally advanced OSCC are surgery, radiation therapy, and chemotherapy [1]. However, with these multimodality treatments, minimal patients have a good survival rate [4]. Therefore, there is a need to develop new treatment strategies that may eventually replace traditional chemotherapy. Recently, nanotechnology can provide drug delivery systems that can minimize nonspecific cell death and maximize the efficacy of traditional therapies [5].

Chitosan (CS) is a biodegradable and biocompatible polysaccharide extracted from crustaceans and is one of the most abundant polymers in nature [6]. In cancer therapy, chitosan nanoparticles (CS NPs) have been used as drug delivery systems [7]. Both hydrophobic and hydrophilic drugs can be delivered by CS NPs owing to the free amine groups, that are present in CS chains and can be used for conjugation with chemotherapeutic agents [8]. The low immunogenicity of CS prevents stimulation of the immune response that could easily eliminate foreign particles from the body [9].

Hyaluronic acid (HA) is a linear polysaccharide formed by N-acetylglucosamine and glucuronic acid units [10]. The cluster of differentiation 44 (CD44) is considered the HA receptor, which is expressed at a low level on the epithelial surface, neuronal, and hematopoietic cells, but is highly expressed in many tumor cells [11]. CD44 expression in HNSCC is the highest relative to other types of cancer where it has a vital role in HNSCC

related to tumor angiogenesis. Hence, targeting CD44 by the action of HA was found to decline the angiogenesis and progression of the tumor [12]. It was found that HA-coated nanoparticles (NPs) have good targeting ability due to passive accumulation and active targeting by the high binding affinity of HA to CD44 receptors in vitro and in vivo [13].

A combination of the positively charged CS NPs and the negatively charged hyaluronic acid nanoparticles (HA NPs) can provide a novel drug delivery system for different types of cancer treatments. It was found that HA-coated CS NPs act as a specific active targeting ligand to CD44 receptors that are overexpressed on tumor cell surfaces [14].

Thymoquinone (TQ), the active chemical constituent of the Nigella Sativa plant, has potent anti-cancer, anti-inflammatory, anti-diabetic, and antioxidant effects [15]. The major drawbacks of TQ are poor bioavailability and hydrophobicity, which delays its therapeutic effect on the targeted site. Hence, various nano drug delivery carriers such as compatible nano lipids and nano polymers have been used with TQ for enhancing its low aqueous solubility and bioavailability [16].

Based on the above knowledge, this study was designed to synthesize TQ-loaded CS NPs followed by surface coating of the formed NPs by HA. Then the cytotoxicity of TQ-loaded CS coated by HA was compared with TQ-loaded CS NPs and free TQ on cancer and normal cell lines to evaluate the efficiency of HA in targeting TQ-loaded CS NPs to cancer cells vs normal cells.

II. Material And Methods

Chemicals and drugs:

Chitosan (Degree of deacetylation: min. 90%, 161 KDa) was purchased from Oxford Lab Fine Chem Llp, Vasai, Maharashtra, India. Hyaluronic acid sodium salt (1.5MDa) was purchased from Fluka, Sigma Aldrich Chemie Gmbh, Buchs, USA. Thymoquinone, Sodium tripolyphosphate (STPP), DAPI (4′,6-Diamidine-2′-phenylindole dihydrochloride) and Fluorescein isothiocyanate isomer were purchased from Sigma Aldrich Chemical Company, Saint Louis, USA. Dulbecco's Modified Eagle's Medium (DMEM), Fetal bovine serum (FBS), and Dulbecco's Phosphate buffered saline (DPBS) were purchased from PAN Biotech, Aidenbach, Germany. Penicillin-streptomycin was purchased from Lonza, Verviers, Belgium. Amphotericin B was purchased from Corning, Manassas, VS, USA. Water soluble tetrazolium (WST-1) reagent was purchased from Abcam, Cambridge, UK. p-Phenylenediamine C6H4(NH2)2 was purchased from PDH Limited, Poole, England.

Drug Synthesis:

I. Preparation of thymoquinone-loaded chitosan nanoparticles:

Thymoquinone-loaded CS NPs were prepared using the ionic gelation (IG) method [17]. Pure TQ (150 mg) was dissolved in 15 ml absolute alcohol and divided into three equal portions. Chitosan (70 mg) was dissolved in 10 ml distilled water containing 1 % ml acetic acid for 30 mins where the first portion of the dissolved TQ was added. 5 ml STPP solution was prepared and added to the second portion of dissolved TQ. The previously prepared mixture was added dropped wisely into the CS beaker and stirred using a magnetic stirrer at room temperature. During the magnetically stirred solution for 1hr, the last portion of the dissolved TQ was added. The prepared formulation containing TQ-CS NPs was centrifuged using a cooling centrifuge at 4° C for 75 minutes at 4500 rpm to collect the pellet of loaded NPs. The collected pellet was suspended in distilled water and freeze-dried to obtain the dried form. The supernatant was collected to detect free TQ using a UV spectrophotometer.

II. Preparation of thymoquinone-loaded chitosan nanoparticles coated by hyaluronic acid:

A portion of TQ-loaded CS NPs (before freeze drying) was suspended in distilled water. Hyaluronic acid (70 mg) was dissolved in a phosphate saline buffer/acetic acid mixture. Hyaluronic acid mixture was added to the suspended NPs' solution and stirred for 90 mins at room temperature on a magnetic stirrer [18]. The prepared TQ-CS-HA NPs were centrifuged using a cooling centrifuge at 4° C for 75 minutes at 4500 rpm, to collect the pellet of TQ-CS-HA NPs. The collected pellet is suspended in distilled water and freeze-dried to obtain the dried form. The supernatant was collected to detect the free HA using High-Performance Liquid Chromatography.

III. Fluorescent labeling of thymoquinone-loaded chitosan nanoparticles coated by hyaluronic acid:

Fluorescein isothiocyanate isomer (FITC) was used to label TQ-CS-HA NPs for evaluation of cellular uptake by CLSM. A small portion of FITC was dissolved in absolute ethanol. A portion of the TQ-CS-HA NPs was suspended in distilled water. Ten ml of the dye-containing solution was added to the suspended NPs solution and stirred at room temperature, at dark, on a magnetic stirrer overnight for 12 hrs. FITC labeled NPs were collected using a cooling centrifuge at 4° C for 75 minutes at 4500 rpm. The collected pellet was washed twice with distilled water then dispersed in distilled water and freeze-dried to obtain the dried form [19].

Characterization of nanoparticles:

I. UV Spectrophotometer analysis of free thymoquinone:

The weight of free TQ in the supernatant of TQ-CS NPs was quantified by using T90+UV-VIS Spectrometer (PG Instruments Ltd). TQ was dissolved in absolute alcohol to prepare five different concentrations that were analyzed at 252 nm, the wavelength of its maximum absorption. The UV–visible spectra analysis of free TQ was taken in absolute ethanol as a solvent. The concentration of unknown free TQ was calculated by comparing its absorbance value with the values of pure TQ in the calibration curve.

II. High-performance liquid chromatography analysis of free hyaluronic acid:

The weight of free HA in the supernatant of TQ-CS-HA NPs was quantified using high-performance liquid chromatography (HPLC) at Nawah Scientific, by Waters 2690 Alliance HPLC system equipped with a Waters 996 photodiode array detector (Waters Corporation, USA). HA stock solution of 2mg/ml in the mobile phase was prepared, then 4 serial dilutions were prepared in concentrations of 1000, 500, 250, and 125µg/ml. Each dilution was filtered using a 0.22µm Nylon syringe filter then 5µl was injected. Chromatographic separation was achieved using Column Xterra RP C18: (250×4.6mm), 5µm. The mobile phase included 0.05 M phosphate buffer with a pH adjusted at 7. The detection was set at 205 nm. The flow rate was maintained at 1ml/min at 50˚C. The mode of elution was isocratic [20]. The percentage of HA that was effectively reacted with TQ-loaded CS NPs was calculated by the following formula [21]: HA (%) = (〖HA〗_(total added)-〖HA〗_free)/〖HA〗_(total added) ×100

where 〖HA〗_(total added) was the amount of polymer used in the coating of TQ loaded CS NPs and 〖HA〗_free was the free HA amount, detected by HPLC into the supernatant volume.

III. Dynamic light scattering (DLS):

The hydrodynamic diameter, polydispersity index (PDI), and zeta potential measurements were performed at room temperature by Zetasizer Nano ZS (Malvern Instruments Ltd, Malvern, UK). The prepared NPs were dispersed into distilled water before measurement. Brownian motion of the NPs causes light to scatter from the particles with different intensities which is detected as a change in light intensity with suitable optics and a photomultiplier. All the data analyses were performed in a triplicate measurement within each run [17].

IV. Fourier transform infrared spectroscopy:

Fourier transform infrared spectroscopy (FTIR) analysis was made to confirm the synthesis of CS NPs and surface modification of CS NPs by HA. It was performed on a Bruker Alpha II FTIR spectrometer (Bruker Corp., Massachusetts, USA). Samples of the prepared NPs (TQ-CS NPs and TQ-CS-HA NPs) after freeze-drying were placed in contact with the surface of the infrared transmitting crystal and examined at a spectral range of 350-8000 cm^{-1}.

V. Transmission electron microscopy (TEM):

The surface morphology and absolute diameter of the prepared NPs (TQ-CS NPs and TQ-CS-HA NPs) were determined by TEM (JEOL JEM-1010). A drop of NPs suspension was placed on a film-coated copper grid, and the excess was removed using filter paper. The copper grid was dried before the examination. JEM-1010 is a high contrast TEM with operating voltage ranges from 40kV to 100kV, equipped with a 2k × 2k AMT CCD camera for digital image acquisition.

Cell culture:

Tissue culture of tongue squamous cell carcinoma cell line (HNO–97) and human normal oral epithelial cell line (OEC) were used in this experiment were obtained from Nawah Scientific, Al-Asmarat, Cairo, Egypt. Both cell lines were cultured in DMEM supplemented with L-glutamine, 4.5 g/L glucose, 10% FBS, 1% penicillin-streptomycin, and 1% amphotericin B at 37°C in a humidified atmosphere of 5 % CO_2 . The serum concentration of treatment media is reduced to 5% since serum proteins may mask the toxicity of the test substance [22].

Cell viability assay:

To evaluate the cytotoxicity of the drugs, free TQ, TQ-CS NPs, and TQ-CS-HA NPs were dissolved in culture media containing 1% DMSO and to make a stock solution with a final concentration of 100 µg/ml followed by four serial dilutions (10 µg/ml, 1 µg/ml, 0.1 µg/ml, 0.01 µg/ml). When the cells reached 80-90 % confluency, they were trypsinized by trypsin-EDTA solution, and fresh growth media was added to collect the cells. The cell suspension was diluted to reach a seeding density of 20,000 cells/ml for HNO-97 and 30,000 cells/ml for OEC. Cell suspension (100µl) was added to each well in a 96-well plate. Plates were incubated in the incubator for 24 hours to ensure cell adherence. After 24 hours of incubation, culture media was removed from the wells. Cells were fed 100µl of treatment media for each well. Plates were incubated for 24h, 48h, and 72h. WST-1 assay protocol was applied according to the manufacturer's instructions. At the end of the drug exposure period, 10 µl of WST-1 reagent was added to each well. Plates were incubated for 0.5-4 hours in the standard culture conditions.

The absorbance of treated and untreated wells was measured using ELISA microplate reader at 450 nm. The percentage of cell viability was calculated using the following equation where OD is the optical density:
Cell viability % = (〖OD〗_(test well)- 〖OD〗_(blank well))/(〖OD〗_(control well)- 〖OD〗_(blank well)) ×100
Half maximal inhibitory concentration (IC_{50}) was calculated for each drug by Graphpad Prism software version 8.0.2, through nonlinear regression analysis using Log (inhibitor) vs. response (three parameters) equation after transformation of all concentrations to Log (concentration). Three values of IC_{50} were calculated for each drug on each day of the experiment.

Morphological changes by inverted phase contrast microscope:
Cells were plated in 12-well plates at a density of 20,000 cells/ well for HNO-97 and 30,000 cells/well for OEC with the respective growth media and incubated overnight. Free TQ, TQ-CS NPs, and TQ-CS-HA NPs (10µg/ml) were added to the cells. After 24 hours, cells were examined and imaged by PCM (Leica Microsystems Ltd.).

In vitro cellular uptake by confocal laser scanning microscope:
Cells were plated on coverslips in 6-well plates at a density of 50,000 cells/ well for HNO-97 and 60,000 cells/well for OEC and incubated overnight. FITC-TQ-CS-HA NPs were added to the wells in a triplicate manner. Cells were fixed at different periods of 1, 2, 3, and 4 hours. After treatment with NPs, the cells were rinsed with DPBS and fixed at room temperature for 20 min in a 4 % paraformaldehyde solution. Cells were permeabilized by immersion in 0.2% Triton X-100 for 5 min. Triton X was aspirated, and cells were rinsed by DPBS. Cells were incubated for 1-5min in Dapi labeling solution at room temperature away from light. Dapi solution was aspirated, and cells were rinsed three times by DPBS. Coverslips were mounted onto microscopic slides with antifade mounting media and the edges of the coverslips were sealed with clear nail varnish [23]. Finally, fluorescence images were acquired using CLSM (Leica TCS SP8). The uptake amount was quantified on the captured images by measuring the NPs' green fluorescence inside cells using ImageJ software.

Statistical analysis:
All data were expressed as mean ± standard deviation using at least three results. One-way ANOVA was applied, followed by Tukey's HSD to detect the statistical significance between IC_{50} of the different drugs, at the same time points, and at different time points for each cell line group. Independent sample T-test was used to detect the significant differences between each drug for the two cell lines at the same time points. The difference was considered significant at p-value < 0.5 Statistical analysis was made by IBM SPSS Statistics version 25 software.

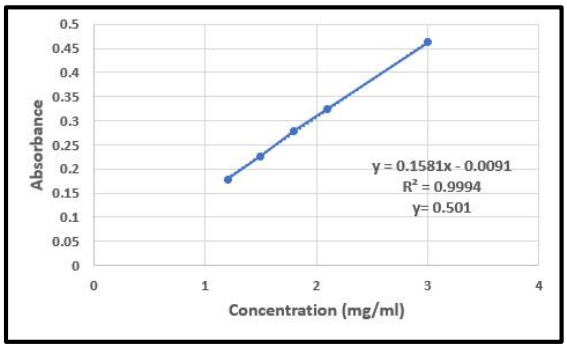

Figure 1: Calibration curve of pure TQ

III. Result

Chemical and physical characterization of the prepared NPs:

I. UV spectrophotometer analysis of free thymoquinone:
The weight of free TQ in the supernatant was calculated after the establishment of a calibration curve obtained by UV spectrophotometer analysis of pure TQ solution in absolute alcohol at 252 nm. The results in **(Fig. 1)** showed linear relation in the range of 1.2 mg/mL–3 mg/mL of TQ with a correlation coefficient of 0.9994. The linear regression equation was y = 0.1581x-0.0091, where y is the absorbance of an unknown concentration of free TQ in the supernatant and x is TQ concentration in mg/ml. Calculation of TQ concentration (x) was 3.21±0.019 mg/ml. The total free TQ in the supernatant was 80.24±0.48 mg. Hence, the weight of TQ loaded on CS NPs was 69.66 ± 0.48 mg.

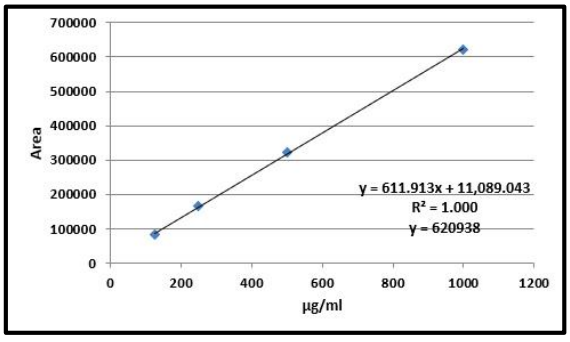

Figure 2: Calibration curve of pure HA

II. HPLC analysis of free hyaluronic acid:
The amount of HA that was effectively bounded with the surface of TQ-CS NPs was determined after the calculation of free HA in the supernatant from the calibration curve **(Fig. 2)** of pure HA that was analyzed by

High-Performance Liquid Chromatography (HPLC). It was linear in the range of 125 µg/mL–1000 µg/mL of HA with a correlation coefficient of 1.000. The linear regression equation was y = 611.913x+11089.043, where y is the area of unknown concentration of free HA in the supernatant and x is HA concentration in µg/ml. The HA concentration (x) was 988.71± 6.87 µg/ml. The total free HA in the supernatant was 31.64±0.296 µg. Hence, the HA that was effectively bounded
to surfaces of TQ-CS NPs was 38.36±0.22 mg.

III. Encapsulation efficiency and loading capacity:

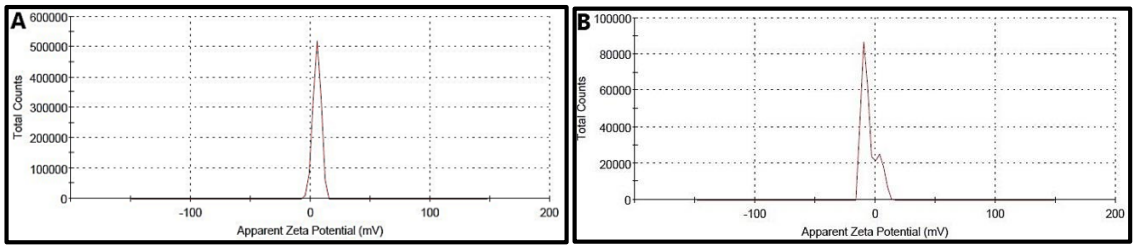

Figure 3: Zeta potential graph of TQ-CS NPs (A) and TQ-CS-HA NPs (B).

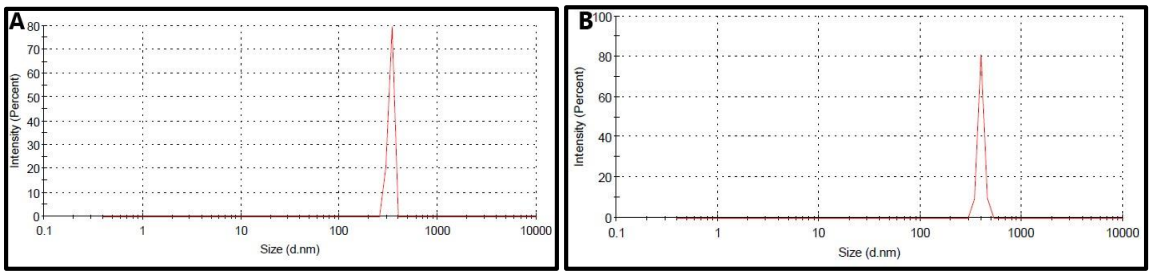

Figure 4: Particle size distribution curve by intensity of TQ-CS NPs (A) and TQ-CS-HA NPs (B).

The TQ encapsulation efficiency for the prepared NPs was 46.51±0.32. The loading capacity for TQ-CS NPs was 43.33±0.30 and for TQ-CS-HA NPs was 24.83±0.17.

IV. Dynamic light scattering:

The mean zeta potentials for TQ-CS NPs and TQ-CS-HA NPs were found to be 6.49 ± 0.24 mV and -5.69 ± 0.30 mV respectively **(Fig. 3. A and B)**. The mean hydrodynamic particle size for the TQ-CS NPs and TQ-CS-HA NPs was found to be 332.4 ± 18.88, and 397.1 ± 25.72 nm, respectively, while the PDI was 0.5 and 0.329, respectively **(Fig. 4A and B)**.

V. Fourier transform infrared spectroscopy (FTIR):

FTIR was performed to compare the functional groups of TQ-loaded CS NPs before and after addition of HA coating as shown in **(Fig. 5A and B).** The peak at 3170.61 cm−1 is the O-H stretch, which overlapped with the N-H_2 stretch from the primary amine groups of CS NPs. This peak was shifted to C-H stretch at 2920.42 cm−1 after HA coating. The peak at 1684.20 cm−1 was C=O, while the peak at 1558.66 cm−1 was C=C. The peak at 1071.17 cm−1was P=O which proved the reaction of inorganic phosphate groups from sodium tripolyphosphate (STPP) with CS. The presence of OH, NH2, and P=O absorption bands confirmed that CS NPs were successfully formed. The appearance of absorption bands at 1558.66 cm−1 and 1684.20 cm−1 that are assigned to the C=C and amide II functional groups, respectively, proved the formation of TQ-loaded CS NPs. In FTIR spectrum of TQ-CS-HA NPs, no new peaks were observed indicating that the coating of CS NPs with HA is due to electrostatic attraction.

VI. Transmission electron microscope (TEM):

TEM images of TQ-CS NPs showed a round and smooth surface in the agglomerated state with 15.3±5.2 nm in absolute diameter **(Fig. 6A).** TQ-CS-HA NPs showed a round surface surrounded by irregular hallo in a well-dispersed form more than TQ-CS NPs with 22.9±6.6 nm in absolute diameter **(Fig. 6B).**

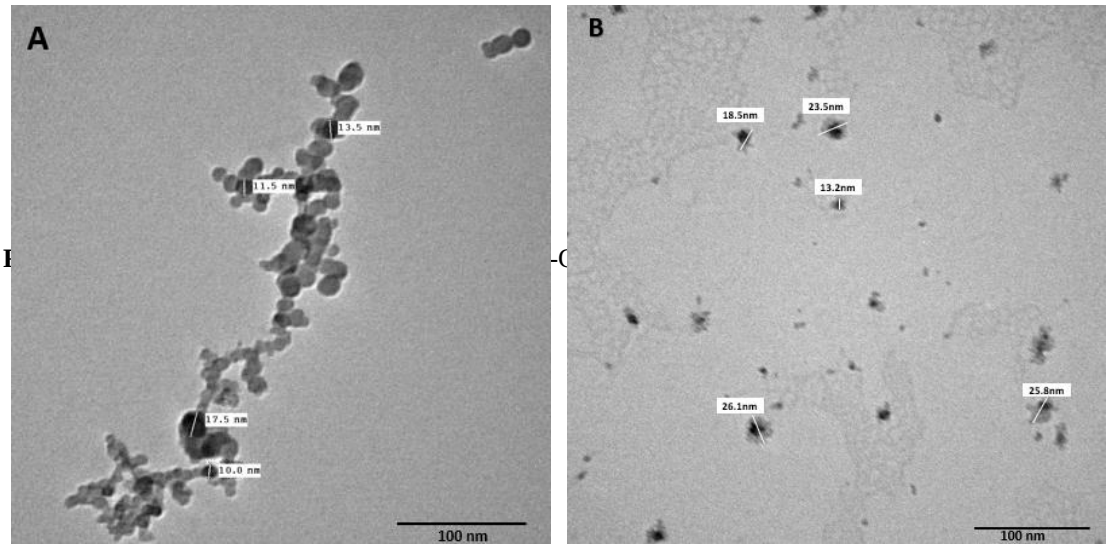

Figure 6: TEM micrograph of TQ-CS NPs (A) and TQ-CS-HA NPs (B).

Cytotoxic effect of nanoparticles on cancer and normal cell lines:

Cellular viability was time and dose-dependent, where the viability was decreased by increasing the concentration of each drug and incubation period on cancer and normal cells **(Fig. 7)**. It was observed that cell viability of OEC cells was much better than HNO-97 cells when treated with nanoformulations of TQ, especially at concentrations 1, 10, and 100µg/ml. Cytotoxicity of free TQ, TQ-CS NPs, and TQ-CS-HA NPs on both cell lines was determined by IC_{50} calculation from 1 to 3 days **(Tab.1).** Regarding the effect of different TQ formulations at the same time point on HNO-97 cells, no statistically significant difference was detected at 24 and 48h while it was significant for TQ and TQ-CS-HA NPs at 72h. There was a statistically significant increase in toxicity of TQ-CS-HA NPs compared to free TQ after 72h. Regarding the effect of different TQ formulations on OEC cells at the same time point, there was a statistically significant decrease in toxicity of the TQ nanoformulations compared to free TQ at 24h and 72h. Considering drug toxicity at 48h, there was only a statistically significant decrease in toxicity of TQ-CS-HA NPs when compared to free TQ **(Fig.8)**. No statistically significant difference was detected regarding the effect of free TQ on the two cell lines upon the 3 days of the experiment. On the other hand, a statistically significant increase in the cytotoxic effect of nanoformulations of TQ was detected on the HNO-97 cell line compared to the OEC cell line upon the 3 days of the experiment **(Fig.9)**.

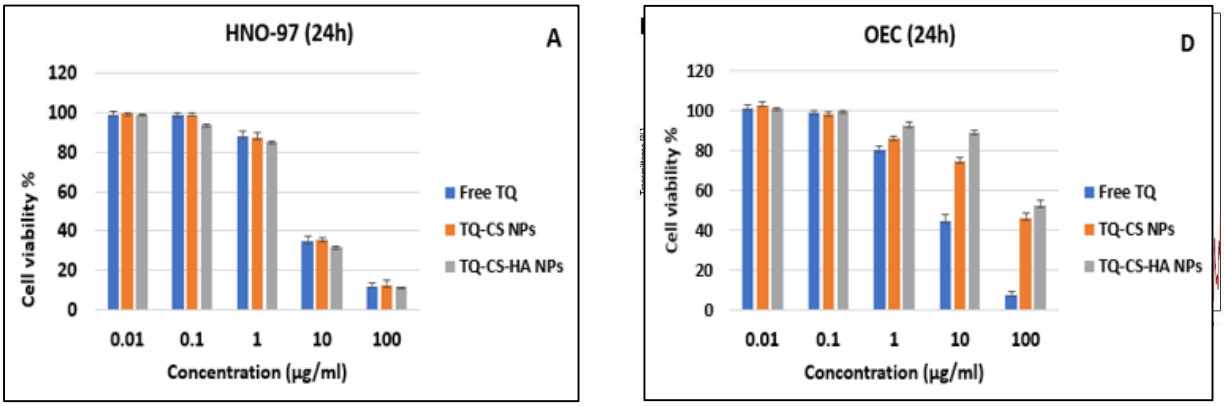

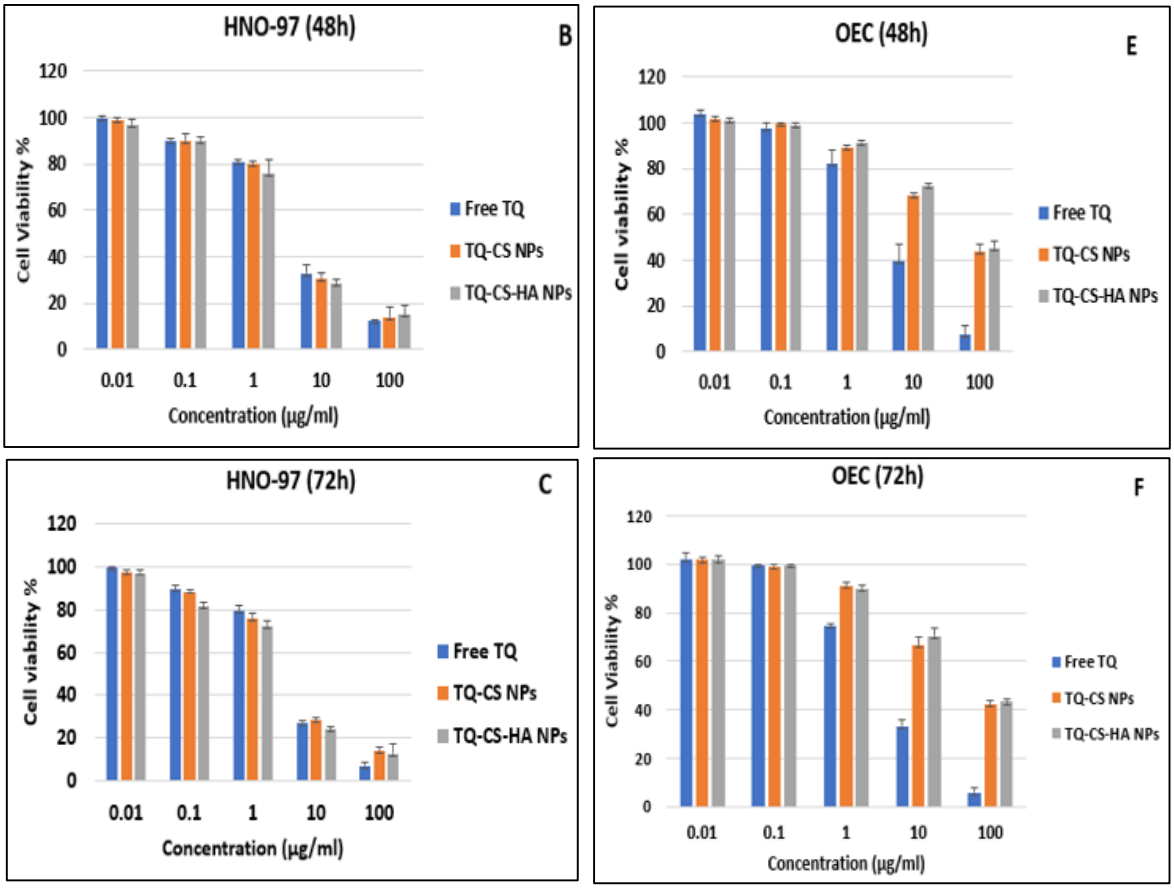

Figure 7: Bar graphs showing cell viability % of HNO-97 (A, B&C) and OEC (D, E&F) cells treated with different concentrations (0.01, 0.1,1,10,100 µg/ml) of free TQ, TQ-CS NPs and TQ-CS-HA NPs for 24, 48 and 72h. Each value represents the mean ± S.D. (n =3).

Table 1: IC_{50} values of the three TQ formulations on cancer and normal cell lines at different times.

Cell lines		**HNO-97**			**OEC**		
Time		**24h**	**48h**	**72h**	**24h**	**48h**	**72**
Drugs							
Free TQ		4.81	4.17	3.81	6.88	5.55	3.3
(IC_{50} µg/ml)		± 0.86	± 0.50	± 0.60	± 1.23	± 1.80	± 0.78
TQ-CS NPs		4.70	3.86	3.01	12.98	8.77	8.38
(IC_{50} µg/ml)		± 0.67	± 0.17	± 0.28	± 3.22	± 2.77	± 2.05
TQ-CS-HA	**NPs**	4.33	3.19	2.63	15.93	11.27	10.47
(IC_{50} µg/ml)		± 0.26	± 1.01	± 0.13	± 1.89	± 1.59	± 1.84

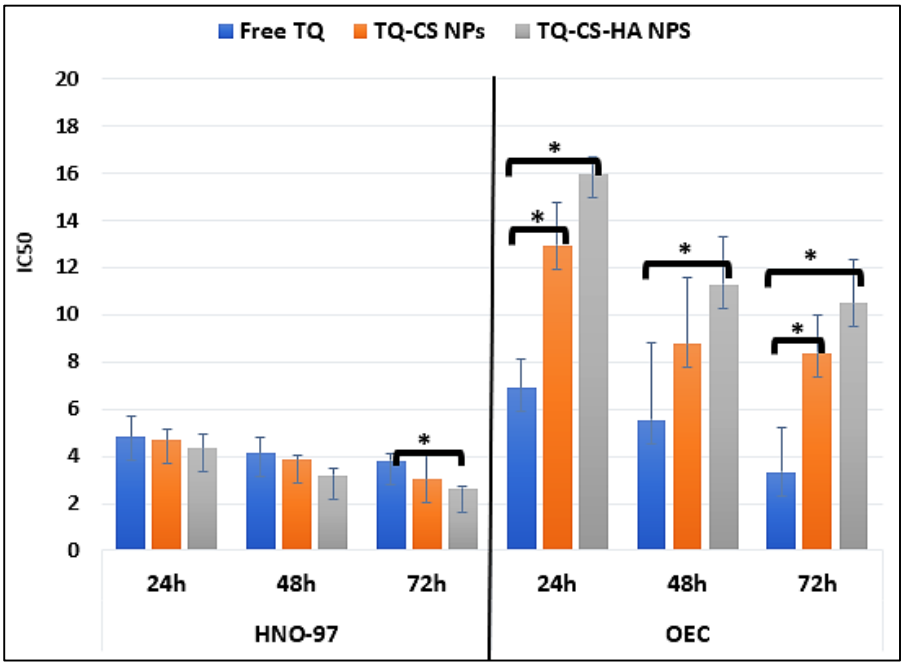

Figure 8: Bar graph showing significant differences between IC_{50} values of three TQ formulations on HNO-97 and OEC cell lines at different time points.
* P-value is considered significant at ≤ 0.05.

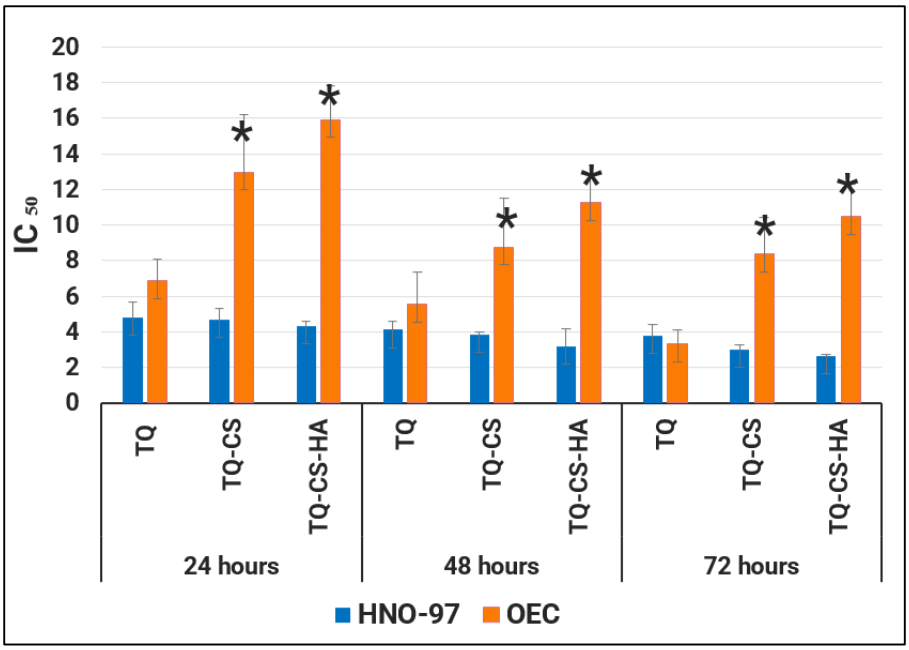

Figure 9: Bar graph showing significant differences between IC_{50} values of three TQ formulations on HNO-97 and OEC cell lines at three days.
* P-value is considered significant at ≤ 0.05.

Effect of free TQ and its nanoformulations on cells' morphology:
The effect of free TQ, TQ-CS NPs, and TQ-CS-HA NPs on cell morphology was assessed by PCM after 24 hours incubation period. PCM images of untreated HNO-97 and OEC cells showed normal two-dimensional monolayer adherent cells with intact plasma and nuclear membranes. There was no chromatin condensation or fragmentation (**Fig. 10 A and 11 A**). PCM images of treated HNO-97 cells showed shrunken poor adherent cells, autophagic cytoplasmic vacuoles, cell membrane blebbing, and apoptotic bodies. Some cells were loosely attached to the

growth surface by extended filopodia and showed a distinct loss of normal cellular morphology **(Fig. 10 B, C, and D)**. PCM images of treated OEC cells showed shrunken poor adherent cells, cell lysis, cell membrane blebbing, apoptotic bodies, as well as chromatin condensation **(Fig. 11 B, C, and D)**.

In vitro cellular uptake assessment of TQ-CS-HA NPs:

The cellular uptake behavior of TQ-CS-HA NPs was investigated by CLSM. It was observed that the strength of green fluorescence intensity of the NPs increased over time from 1h to 4h in both cell lines. The NPs were more dispersed within the cells after 1h and 2h, while by the increasing time more agglomerated NPs appeared within the cells indicating that cellular uptake increased over time. Moreover, the fluorescence intensity of the NPs was stronger within HNO-97 cells compared to OEC cells, especially after 3 and 4 hours **(Fig. 12 and 13)**, demonstrating higher uptake of TQ-CS-HA NPs by HNO-97 cells compared to OEC cells. Fluorescence intensity/cell obtained by J software demonstrated a significant increase in intensity within HNO-97 cells compared to OEC cells after 1, 3, and 4 hours **(Fig. 14).**

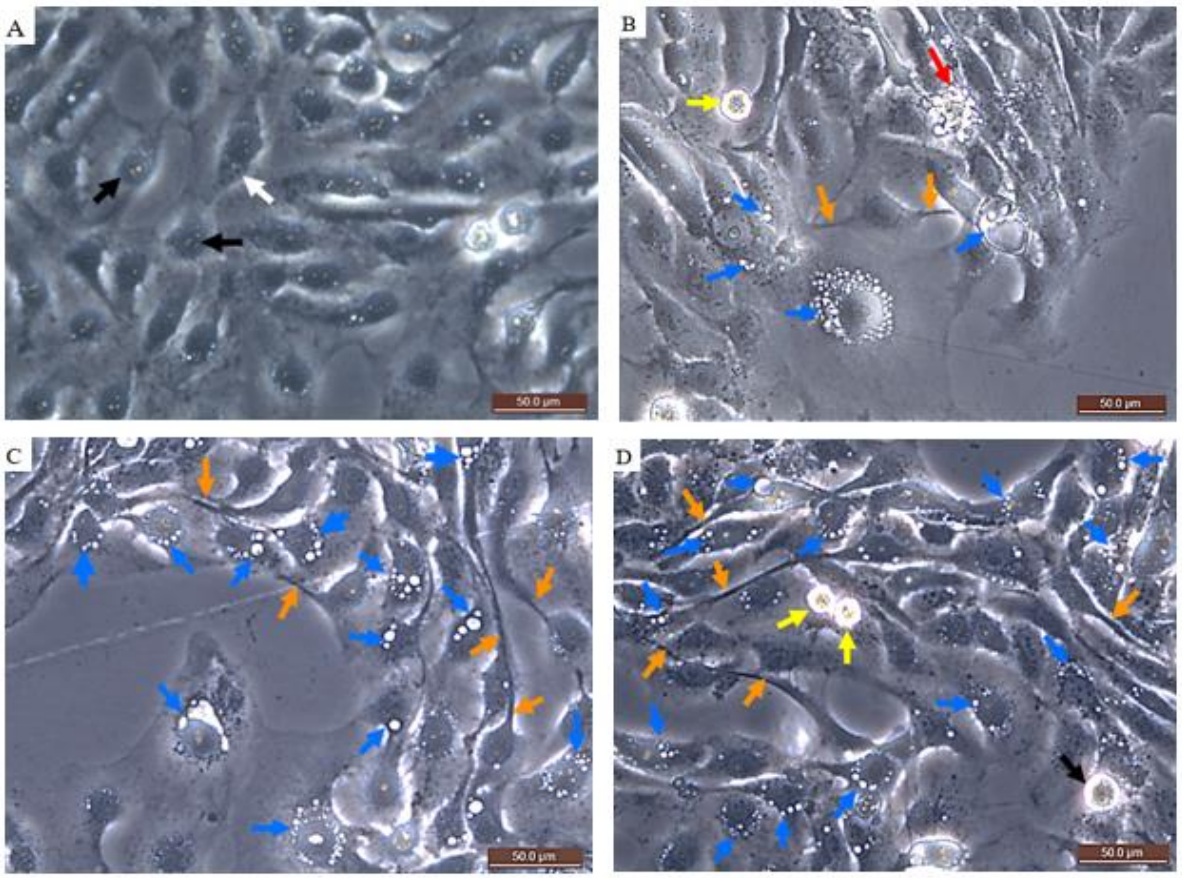

Figure 10: Phase contrast micrograph imaging of untreated (A) and treated HNO-97 cells by free TQ (B), TQ-CS NPs (C), and TQ-CS-HA NPs (D) showing normal morphological structure of adherent cells with intact plasma (white arrows), nuclear membranes (black arrows), cell membrane blebbing in apoptotic cell (red arrow), cytoplasmic vacuolization (blue arrow), filopodia (orange arrow), apoptotic body (yellow arrow), and replicating cell with smooth cell membrane and normal condensing chromatin in mitosis phase (black arrow), (magnification ×40).

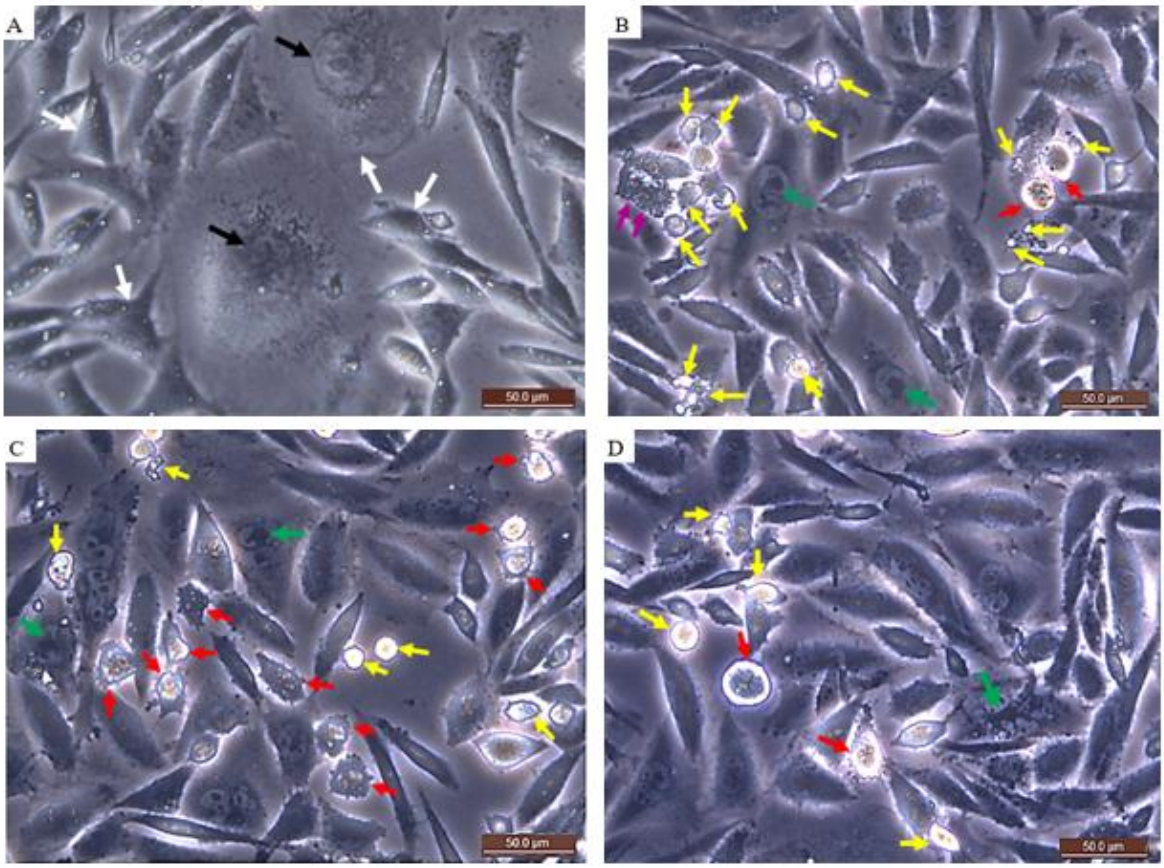

Figure 11: Phase contrast microscope imaging of untreated (A) and treated OEC cells by free TQ (B), TQ-CS NPs (C), and TQ-CS-HA NPs (D) showing normal morphological structure of adherent cells with intact plasma (white arrows) and nuclear membranes (black arrows), blebbing and irregular plasma membrane in apoptotic cells (red arrows), apoptotic bodies (yellow arrows), condensed chromatin (green arrows) and cell lysis (purple arrows), (magnification ×40).

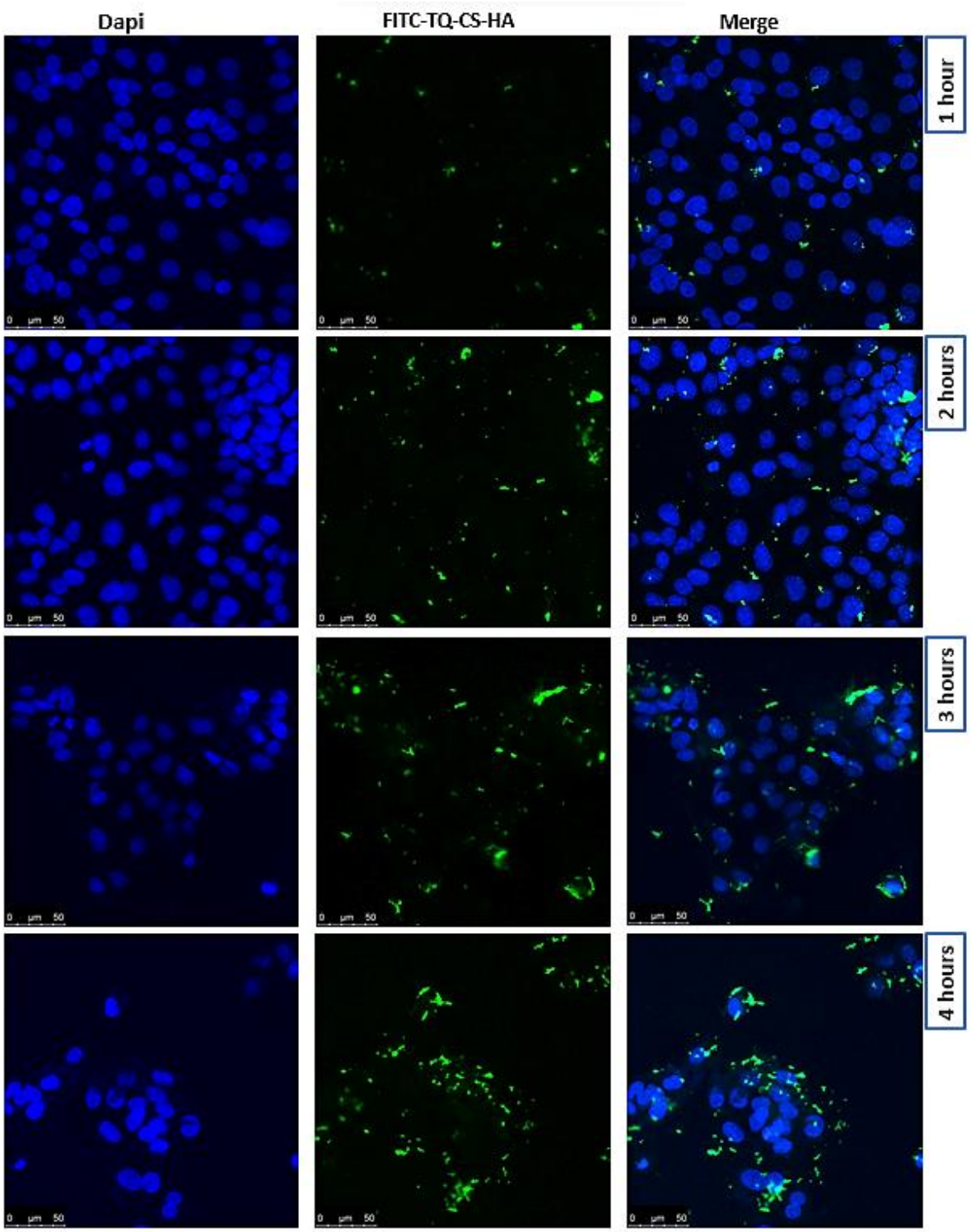

Figure 12: CLSM images of HNO-97 cells after incubation with FITC-TQ-CS-HA NPs (10µg/ml) for 1h, 2h, 3h and 4h. The nuclei stained with DAPI were observed as blue fluorescence. The NPs were observed as green fluorescence. The intensity of green fluorescence increased by time.

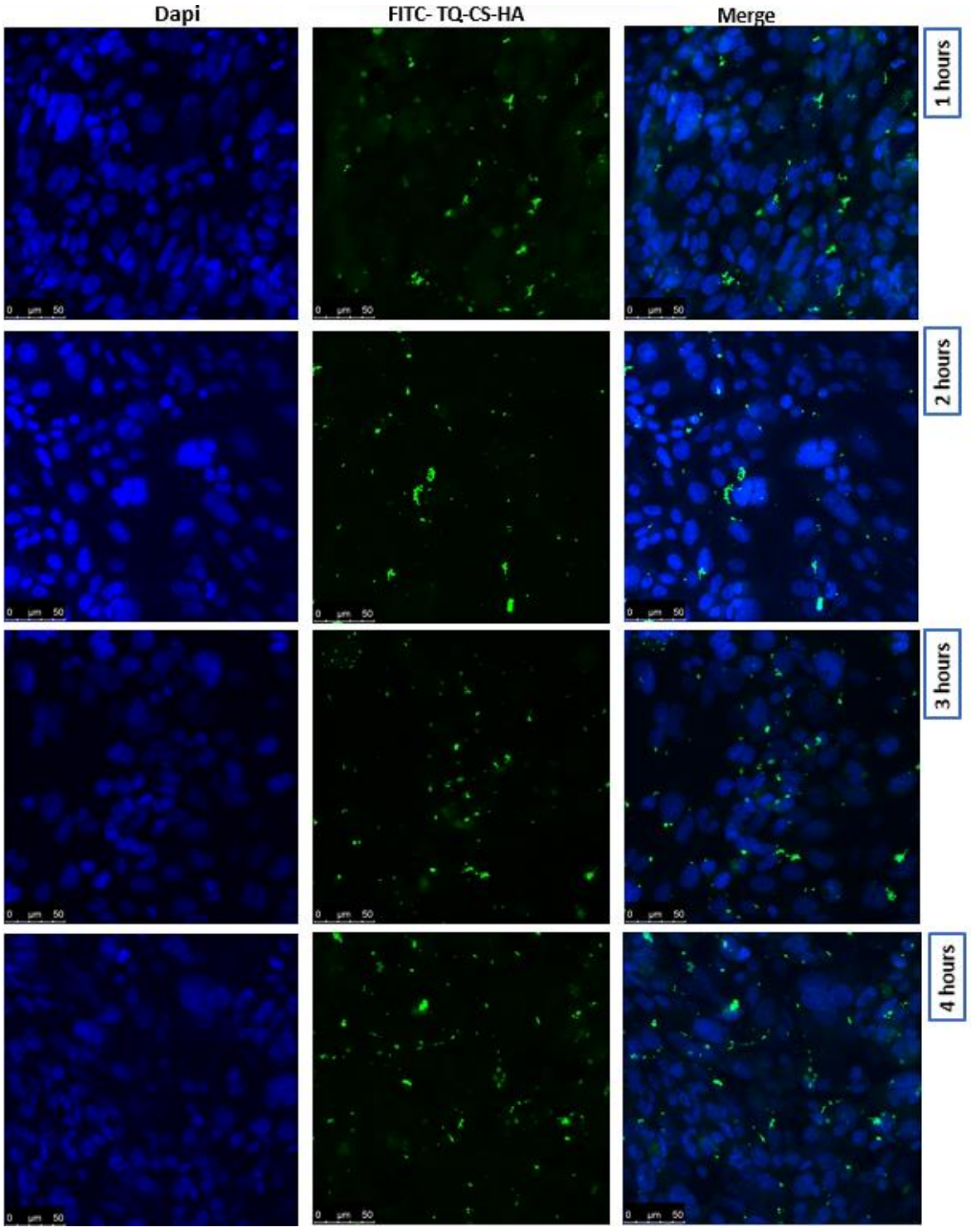

Figure 13: CLSM images of OEC cells after incubation with FITC-TQ-CS-HA NPs (10µg/ml) for 1h, 2h, 3h, and 4 h. The nuclei stained with DAPI were observed as blue fluorescence. The NPs were observed as green fluorescence. The intensity of green fluorescence increased by time.

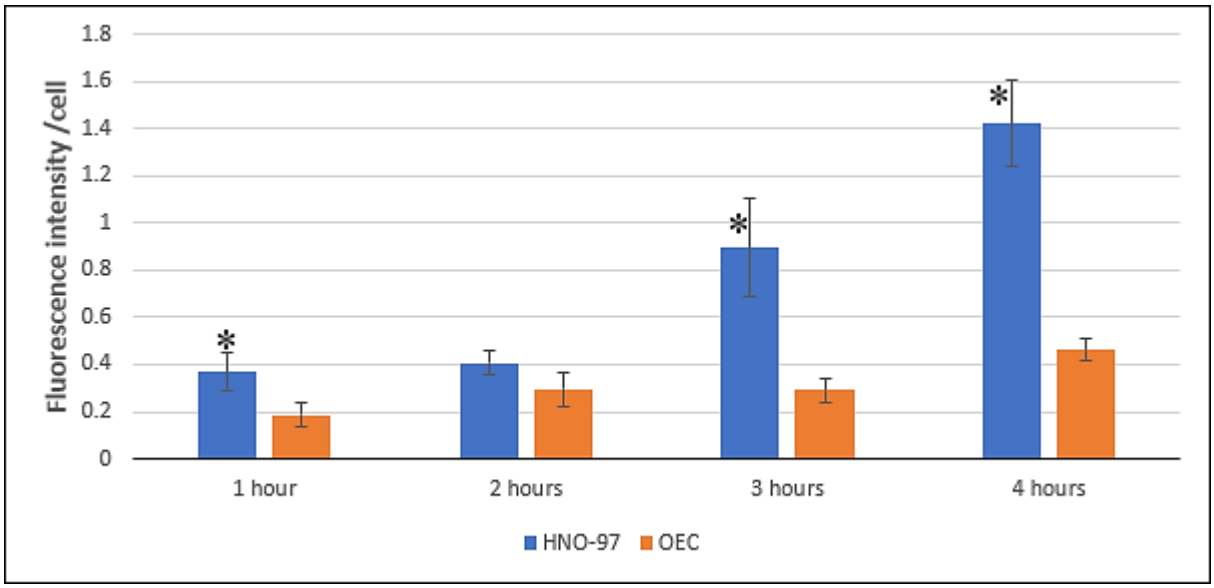

Figure 14: Bar graph showing mean fluorescent intensity of FITC-TQ-CS-HA NPs (10µg/ml) on HNO-97 and OEC cells after 1, 2, 3 and 4 hours of incubation. Results are presented as mean ± S.D, (n=3). Differences between groups were assessed by independent sample T-test at *P ≤ 0.05. Values of fluorescence intensity were obtained by image J software.

IV. Discussion

Targeted therapy in HNSCC is getting great attention to diminish the drawbacks of available traditional therapy [24] The purpose of this study was to evaluate the efficiency of HA in targeting TQ-CS NPs to the OSCC cells with minimal toxicity on normal oral epithelial cells.

TQ, the active constituent of Nigella Sativa, was used in an attempt to provide a safer, more effective, and more reasonable drug for OSCC [25]. CS is one of the most used polymer nanocarriers with different types of chemotherapy and phytochemicals. Chitosan NPs can overcome the drawbacks of TQ [26]. In addition, surface modification of CS NPs by HA can enhance its effect and targeting ability [27], where HA-CD44 interaction can decrease toxicity, enhance cellular uptake, and modulate the immune response against the NPs in cancer treatment due to its high affinity to CD44 receptors [28].

The results revealed that the cell viability of both cell lines was time and dose-dependent, where the viability was decreased by increasing the concentration of each drug and incubation period. The cell viability of OEC cells was much better than HNO-97 cells when they were treated with TQ nanoformulations. Cytotoxicity of all TQ formulations was time-dependent on both cell lines, where IC_{50} values were decreasing with time.

The cytotoxic effect of TQ against OEC cells was not significantly different compared to its effect on HNO-97 cells. On contrary, Alaufi et al. found that cytotoxicity of free TQ was higher in human OSCC cell line compared to normal OEC cell line [29]. The present findings showed the toxicity of TQ increased against OEC cells after 72h when compared with the first day. This is most probably related to the low proliferation rate of the normal cells compared to cancer cells as was observed in this experiment. The low serum level of the treatment media might affect cell viability, in addition to the drug effect [30].

Cytotoxicity of TQ-CS NPs on OEC cells was statistically significantly lower than the toxicity of free TQ at the same time point. Also, there was a statistically significant increase in cytotoxicity of TQ-CS NPs on HNO-97 cells compared to OEC cells during the three days of the experiment. These results were comparable to the results of Anitha et al., who found that the normal cells showed higher viability with curcumin-loaded CS NPs compared to free curcumin [31]. The sensitivity of cancer cells to positively charged CS NPs could be attributed to the generation of more negative charges on the cell membrane of cancer cells while the surfaces of normal cells are neutral or slightly positive [32]. Increasing cytotoxicity of TQ-CS NPs by the time on HNO-97 and OEC cells may indicate sustained release of the drug from the NPs [31].

In the present study, TQ-CS-HA NPs showed a significant increase of cytotoxicity on HNO-97 cells when compared to free TQ after 72h, while their cytotoxicity on OEC cells was significantly decreased compared to free TQ at the three days. Moreover, they had a significant increase in cytotoxicity on HNO-97 cells compared to OEC cells at three days. These results were comparable to Thomas et al., findings who used paclitaxel-loaded HA micelles for targeting HNSCC (SCC7) in vitro and xenograft tumor of SCC7 in athymic nude mice. They

found that the targeted nano micelles achieved a visible decrease in cell viability in the HNSCC cell line as compared to free paclitaxel with minimal toxicity on normal fibroblast cells [33].

Other studies confirmed the effectiveness of HA-coated CS NPs in targeting different tumors with different chemotherapeutic agents. Shabani Ravari et al. used CS-coated HA NPs for effective targeting of docetaxel to breast cancer cell lines [34]. Another study by Wang et al. confirmed the same results when using HA-coated CS NPs to promote the delivery of 5-fluorouracil into tumor cells that highly express CD44 [14]. Later, a study by Zhang et al. reported similar results when they used HA-coated CS NPs for active targeting of paclitaxel to breast cancer in vitro and in vivo. They concluded that the effectiveness of HA-coated NPs, as a drug carrier, is related to the ability of HA to active targeting the modified drug-loaded NPs, as they can recognize and internalize into the tumor cells through receptor-mediated endocytosis [35]. Choi et al. added that the loaded drug in the modified NPs can be released inside the tumor cells. In the case of the drug-loaded NPs without surface modification, only a fraction of the released drug is delivered to the target site of tumor cells [13].

Results of the morphological changes in cancer and normal cells were observed and showed that free TQ and its nanoformulations can induce morphological features of different forms of cell death (apoptosis, necrosis, and autophagy). TQ had resulted in autophagic vacuoles and features of apoptosis in HNO-97 cells, consistent with a previous study by Chu et al., they reported that TQ could induce apoptosis and autophagy in HNSCC cell line via caspase activation and light chain3-II activation, respectively [36]. Normal OEC cells, in the present study, showed features of apoptotic cell death and cell lysis resulting from necrosis. Alaufi et al. found that TQ induced significant apoptotic effects in cancer cells as well as the apoptotic and necrotic effects in normal cells after 24h. Furthermore, they found that TQ significantly increased the expression of the pro-apoptotic protein (caspase-9) and decreased expression of the anti-apoptotic protein (Bcl-2) in cancer and normal cells. On the other hand, TQ had significantly increased expression of the pro-apoptotic protein (p53) in normal cells as well [32].

Findings of the WST-1 assay were confirmed with CLSM, where the fluorescence intensity of FITC-TQ-CS-HA NPs was significantly higher in HNO-97 cells more than in OEC cells after 1, 3, and 4h. These data indicated that HA-coated NPs were taken up to a greater extent by HNO-97 cells because HA targeting to specific receptors. Choi et al. used CLSM to verify the ability of HA for targeting the SCC cell line (SCC7) more than normal fibroblast cells and found similar results [13]. Moreover, a study by Zhang et al. confirmed our results by using CLSM and reported the high cellular uptake of HA-coated CS NPs by the cancer cells contrary to human umbilical vein endothelial cells [35]. Despite CD44 receptors being expressed on both normal and tumor cells, HA-coated NPs effectively target cancer cells more than normal cells. The reason is that these receptors are endogenously expressed with low levels and require activation in normal cells, while in cancer cells they do not need activation due to their high expression and high affinity to HA, especially in rapidly growing tumors [37].

V. Conclusion

Coating of TQ-CS NPs by HA was fabricated successfully as confirmed by TEM, HPLC, FTIR, and zeta potential. TQ-CS-HA NPs showed higher cytotoxicity to HNO-97 cells and lower cytotoxicity to OEC compared to free TQ. In addition, TQ-CS-HA NPs were more cytotoxic to HNO-97 cells than OEC cells. The enhanced cellular uptake of TQ-CS-HA NPs into HNO-97 cells rather than OEC cells was confirmed by CLSM imaging. Hence, CS-HA NPs could provide a safer and more effective drug delivery system than CS NPs..

References

[1]. Johnson DE, Burtness B, Leemans CR, Lui VWY, Bauman JE, Grandis JR. Head and neck squamous cell carcinoma. Nat Rev Dis Primers 2020;6:1–22.
[2]. Sung H, Ferlay J, Siegel RL, Laversanne M, Soerjomataram I, Jemal A, et al. Global cancer statistics 2020: globocan estimates of incidence and mortality worldwide for 36 cancers in 185 countries. CA Cancer J Clin 2021;71:209–49.
[3]. Patterson RH, Fischman VG, Wasserman I, Siu J, Shrime MG, Fagan JJ, et al. Global burden of head and neck cancer: economic consequences, health, and the role of surgery. Otolaryngology - Head and Neck Surgery 2020;162:296–303.
[4]. Hartner L. Chemotherapy for oral cancer. Dent Clin North Am 2018;62:87–97.
[5]. Gharat SA, Momin M, Bhavsar C. Oral squamous cell carcinoma: Current treatment strategies and nanotechnology-based approaches for prevention and therapy. Crit Rev Ther Drug Carrier Syst 2016;33:363–400.
[6]. Yanat M, Schroën K. Preparation methods and applications of chitosan nanoparticles; with an outlook toward reinforcement of biodegradable packaging. React Funct Polym 2021;161:104849.
[7]. Zhang H, Wu F, Li Y, Yang X, Huang J, Lv T, et al. Chitosan-based nanoparticles for improved anticancer efficacy and bioavailability of mifepristone. Beilstein Journal of Nanotechnology 2016;7:1861–70.
[8]. Babu A, Ramesh R. Multifaceted applications of chitosan in cancer drug delivery and therapy. Mar Drugs 2017;15:1–19.
[9]. Jayakumar R, Menon D, Manzoor K, Nair S v., Tamura H. Biomedical applications of chitin and chitosan based nanomaterials - A short review. Carbohydr Polym 2010;82:227–32.
[10]. Huang G, Chen J. Preparation and applications of hyaluronic acid and its derivatives. Int J Biol Macromol 2019;125:478–84.
[11]. Jong A, Wu CH, Gonzales-Gomez I, Kwon-Chung KJ, Chang YC, Tseng HK, et al. Hyaluronic acid receptor CD44 deficiency is associated with decreased cryptococcus neoformans brain infection. Journal of Biological Chemistry 2012;287:15298–306.
[12]. Ludwig N, Szczepanski MJ, Gluszko A, Szafarowski T, Azambuja JH, Dolg L, et al. CD44(+) tumor cells promote early angiogenesis in head and neck squamous cell carcinoma. Cancer Lett 2019;467:85–95.
[13]. Choi KY, Chung H, Min KH, Yoon HY, Kim K, Park JH, et al. Self-assembled hyaluronic acid nanoparticles for active tumor targeting. Biomaterials 2010;31:106–14.

[14]. Wang T, Hou J, Su C, Zhao L, Shi Y. Hyaluronic acid-coated chitosan nanoparticles induce ROS-mediated tumor cell apoptosis and enhance antitumor efficiency by targeted drug delivery via CD44. J Nanobiotechnology 2017;15:1–12.
[15]. Ahmad A, Mishra RK, Vyawahare A, Kumar A, Rehman MU, Qamar W, et al. Thymoquinone (2-Isoprpyl-5-methyl-1, 4-benzoquinone) as a chemopreventive/anticancer agent: Chemistry and biological effects. Saudi Pharmaceutical Journal 2019;27:1113–26.
[16]. Negi P, Rathore C, Sharma G, Singh B, Katare OP. Thymoquinone a Potential therapeutic molecule from the plant nigella sativa: role of colloidal carriers in its effective delivery. Recent Pat Drug Deliv Formul 2018;12:3–22.
[17]. Alam S, Khan ZI, Mustafa G, Kumar M, Islam F, Bhatnagar A, et al. Development and evaluation of thymoquinone-encapsulated chitosan nanoparticles for nose-to-brain targeting: A pharmacoscintigraphic study. Int J Nanomedicine 2012;7:5705–18.
[18]. Dhamane SP, Jagdale SC. Development of rifampicin loaded hyaluronic acid coated chitosan nanoparticles. European Journal of Molecular and Clinical Medicine 2020;7:3447–58.
[19]. Huang M, Ma Z, Khor E, Lim LY. Uptake of FITC-chitosan nanoparticles by A549 cells. Pharm Res 2002;19:1488–94.
[20]. El-Behairy M, Taher M, Abdallah I. Straightforward determination of sodium hyaluronate in active pharmaceutical ingredient and ophthalmic formulations: validation and stability study. Journal of Advanced Pharmacy Research 2020;4:147–52.
[21]. Chiesa E, Dorati R, Conti B, Modena T, Cova E, Meloni F, et al. Hyaluronic acid-decorated chitosan nanoparticles for CD44-targeted delivery of everolimus. Int J Mol Sci 2018;19:2310.
[22]. Meerloo J van, Kaspers GJL, Cloos J. Cell Sensitivity Assays. In: Cree IA, editor. Cancer Cell Culture: Methods and Protocols. 2nd Edition, Humana Press; 2011, p. 237–46.
[23]. Chazotte B. Labeling nuclear DNA using DAPI. Cold Spring Harb Protoc 2011;6:80–3.
[24]. Liu L, Chen J, Cai X, Yao Z, Huang J. Progress in targeted therapeutic drugs for oral squamous cell carcinoma. Surg Oncol 2019;31:90–7.
[25]. Ballout F, Habli Z, Rahal ON, Fatfat M, Gali-Muhtasib H. Thymoquinone-based nanotechnology for cancer therapy: promises and challenges. Drug Discov Today 2018;23:1089–98.
[26]. Sonin D, Pochkaeva E, Zhuravskii S, Postnov V, Korolev D, Vasina L, et al. Biological safety and biodistribution of chitosan nanoparticles. Nanomaterials 2020;10:1–23.
[27]. Wang JJ, Zeng ZW, Xiao RZ, Xie T, Zhou GL, Zhan XR, et al. Recent advances of chitosan nanoparticles as drug carriers. Int J Nanomedicine 2011;6:765–74.
[28]. Sanità G, Carrese B, Lamberti A. Nanoparticle surface functionalization: how to improve biocompatibility and cellular internalization. Frontiers in Molecular Bioscience 2020;7:587012.
[29]. Alaufi OM, Noorwali A, Zahran F, Al-Abd AM, Al-Attas S. Cytotoxicity of thymoquinone alone or in combination with cisplatin (CDDP) against oral squamous cell carcinoma in vitro. Sci Rep 2017;7:1–12.
[30]. Rashid M ur, Coombs KM. Serum-reduced media impacts on cell viability and protein expression in human lung epithelial cells. J Cell Physiol 2019;234:7718–24.
[31]. Anitha A, Maya S, Deepa N, Chennazhi KP, Nair S v., Jayakumar R. Curcumin-loaded N, O-carboxymethyl chitosan nanoparticles for cancer drug delivery. J Biomater Sci Polym Ed 2012;23:1381–400.
[32]. Chen B, Le W, Wang Y, Li Z, Wang D, Ren L, et al. Targeting negative surface charges of cancer cells by multifunctional nanoprobes. Theranostics 2016;6:1887–98.
[33]. Thomas RG, Moon M, Lee S, Yeon Y. Paclitaxel loaded hyaluronic acid nanoparticles for targeted cancer therapy: In vitro and in vivo analysis. Int J Biol Macromol 2015;72:510–8.
[34]. Shabani Ravari N, Goodarzi N, Alvandifar F, Amini M, Souri E, Khoshayand MR, et al. Fabrication and biological evaluation of chitosan coated hyaluronic acid-docetaxel conjugate nanoparticles in CD44+ cancer cells. DARU, Journal of Pharmaceutical Sciences 2016;24:1–12.
[35]. Zhang X, Niu S, Williams GR, Wu J, Chen X, Zheng H, et al. Dual-responsive nanoparticles based on chitosan for enhanced breast cancer therapy. Carbohydr Polym 2019;221:84–93.
[36]. Chu SC, Hsieh YS, Yu CC, Lai YY, Chen PN. Thymoquinone induces cell death in human squamous carcinoma cells via caspase activation-dependent apoptosis and LC3-II activation-dependent autophagy. PLoS One 2014;9:e101579.
[37]. Misra S, Hascall VC, Markwald RR, Ghatak S. Interactions between hyaluronan and its receptors (CD44, RHAMM) regulate the activities of inflammation and cancer. Front Immunol 2015;6:201.